CHAPTER 5

POLYANILINE INTERCALATED VANADIUM PENTOXIDE NANOSHEETS FOR THE IMPROVEMENT OF LUBRICITY OF BASE OIL

Conventional additives considerably improve the tribological behavior of the base oil at higher additive concentrations. They have numerous technical drawbacks, such as failure at high pressure and temperature, high reactivity, inherent toxicity, ineffectiveness at low temperatures, and non-biodegradability. This has sparked a desire to create environment-friendly nano-lubricants that would improve tribo-pair performance having significant implications for emission reduction, environmental protection, and energy conservation, thus, less harmful to the environment. Nano lubricants are stable colloidal suspensions of nano-sized substances like nanoparticles, nanotubes, nanofibers, nanorods, nanosheets, and nanowires added in a minimum quantity to base oil, but improving the tribological activity to a greater extent [Paul et al. (2019)]. Such systems have enhanced thermal conductivity, which helps remove heat produced from excessive wear and friction. Compared to lubricants dispersed with micro-sized particles, nanoparticle-laden lubricants offer much better stability. The factors like base fluids, nano-sized additives, stability enhancement, surfactant concentrations, preparation techniques, and conventional and novel test approach significantly impact the tribological properties of nano lubricants [Wang et al. (2022)]. Added nanoparticles become more chemically reactive because of their vast surface area to volume ratio, which helps modify the nanoparticle surface while enhancing their agglomerating tendencies and reducing their dispersibility in the base oil [Paul et al. (2019)]. The functionalization of the surface of nanoparticles inhibits their aggregation in the non-polar base oil and increases the stability of the dispersion in oil, thereby enhancing their tribological properties. Two-dimensional (2D) nanomaterials like graphene, molybdenum disulfide, graphitic carbon nitride, hexagonal boron nitride, etc., show lubricating behavior because of weak van der Waals forces between adjacent

layers. These materials have a substantially higher specific surface area than other nano-structured materials. Therefore, they can reduce the likelihood of coming into touch with rubbing surfaces directly and the amount of friction between them [Rao et al. (2014), Xiao et al. (2017)].

Given the above, it appeared enthralling to investigate tribological properties of paraffin oil-based nano lubricants containing nanoparticles and/ or 2D- nanomaterials.

Vanadium pentoxide (V_2O_5), an n-type semiconductor [Kundu et al. (2017)], has been used as a counter electrode in dye-sensitized solar cells [Gnanasekar et al. (2021)], sensing materials for gases [Schneider et al. (2016)], supercapacitor electrodes [Boukhalfa et al. (2012)], cathode materials for both lithium-ion as well as zinc-ion batteries [Kou et al. (2021), Javed et al. (2020)] and catalysts /photocatalysts [Wan et al. (2021), Jianhua et al. (2006)] in several reactions. It has also found applications in wastewater treatment, biomedical [Karthik et al. (2019)], optical [Zou et al. (2009)], and electronic fields [Yazdi et al. (2021)]. Vanadium oxide (V_2O_5) is one of the potential lubricious oxides used as a solid lubricant [Huang et al. (2016)]. The multiple layers of V_2O_5 are piled up through van der Waals forces. Its low friction is due to the crystallographic slip system [Dai et al. (2017)]. Since it is not that hard and wear-resistant, silicon is added to V_2O_5 coatings [Mirabal-Rojas et al. (2018)], or vanadium is usually added into hard nitride coatings [Fateh et al. (2008)], iron-based arc sprayed coatings [Tillmann et al. (2019)] that could eventually form self-lubricating V_2O_5 layer on heating. V_2O_5 nanowires have been particularly used in metal matrix composites like TiAl [Yang et al. (2016)], and NiAl [Ibrahim et al. (2019)] to decrease the wear rate and coefficient of friction and increase hardness. V_2O_5 nanoparticles interacted with pure aluminum forming an Al-Al_2O_3

composite in situ, reducing friction and wear [Singla et al. (2015)].The friction and wear-reducing performance of the nickel aluminum matrix solid lubricating composite was further improved by silver and silver vanadate [Zhu et al. (2019)].

Polyaniline (PANI), a p-type organic semiconductor, is recognized very well as a compatible conducting polymer [Kundu et al. (2017), Yakuphanoglu et al. (2007)]. Its striking attributes; high electrical and thermal conductivity, environmental stability, redox behavior, and inexpensive facile synthesis make it a versatile material in different fields such as supercapacitors [Cong et al. (2013)], biosensors [Kazemi et al. (2021)], giant magnetoresistance sensors [Gu et al. (2018)], photovoltaic cells [Bejbouji et al. (2010)], light-emitting diodes [Yakuphanoglu et al. (2007)] actuators [Gao et al. (2003)], field-effect transistors [Lee et al. (2009), Chen et al. (2011)], biofuel cells [Han et al. (2006), Inamuddin et al. (2019)],corrosion protection [Hafeez et al. (2017)], rechargeable batteries [Ghanbari et al. (2006), Jiménez et al. (2017)], membranes [Feng et al. (2008), Razali et al. (2013)], solar-cell devices [Wang et al. (2007)], electromagnetic interference shielding [Qiu et al. (2018)], advanced drug delivery systems [Svirskis et al. (2010)], metamaterials [Xu et al. (2020)], coupling agents [Gu et al. (2018)], and catalysts [Setyowati et al. (2020), Sonawane et al. (2021)] etc. The skeleton of PANI is made up of a delocalized conjugated system of benzenoid and quinoid forms. It has three interconvertible redox states; completely reduced colorless leucoemeraldine, completely oxidized purple pernigraniline, and partially oxidized blue emeraldine. Out of these, emeraldine base is recommended as the most effective form since its interaction with an acid yields green-colored emeraldine salt, which shows very high electrical conductivity due to the delocalized π-bonds throughout the polymeric system [Gu et

al. (2018)]. Besides chemical methods [Alemayehu et al. (2014)], emeraldine salt (PANI) can be synthesized electrochemically as well [Bhadra et al. (2007)]. Leucoemeraldine and pernigraniline are poor conductors, even after interaction with an acid [Vyas et al. (2017)]. The widespread use of PANI is acknowledged owing to its high conductivity in preparing conductive composites. Cao et al. studied corrosion resistance and tribological characteristics of ionic liquids doped PANI as lubricant additives to different greases [Cao et al. (2020)]. Tribo-active performance of a composite of PANI with graphene oxide (PANI-GO) in liquid paraffin was investigated by Lieu and associates [Liu et al. (2018)]. Fan and collaborators synthesized polyaniline-coated (3-aminopropyl) core-shell particles of triethoxysilane-modified β-Si_3N_4 (m-SiN @ PANI) and applied them to upgrade the tribological properties of a phenolic resin/carbon fiber composite [Fan et al. (2019)]. Corrosion prevention and wear-reducing properties of PANI/graphene epoxy-coated Mg-9Li-5Al-3Sn-1Zn, and Mg-9Li-7Al-1Sn alloys have been reported in the marine environment [Maurya et al. (2019)].

As discussed above, most of the work on V_2O_5 is focused on metal matrix composites where wear and friction have been evaluated in the dry state. The nano lamellar structures like reduced graphene oxides (rGO) [Jaiswal et al. (2016), Verma et al. (2018), Verma et al. (2020b)], graphitic-carbon nitride (g-C_3N_4) [Singh et al. (2021)], molybdenum disulfide (MoS_2) [Shukla et al. (2020)] have been used by us as tribologically active additives in a base oil, V_2O_5 nanosheets are also expected to be used for the same purpose. A report by Dai et al. (2017) shows that the tribological activity of hydrothermally prepared V_2O_5 nanosheets has been studied as an additive to a mineral oil using a pin-on-disk tribometer. The friction behavior has been evaluated in all the lubrication regimes using rotational mode under 0.15–1

N loads at sliding speeds of 0.004–0.4 m/s. A wear test has been performed in the boundary lubrication regime via reciprocating sliding mode at 5 N (1GPa) load, 1 Hz oscillation frequency, the length of wear track as10 mm, and a total sliding distance of 5000 m. It motivated us to prepare nano lamellar V_2O_5 ultrasonically by exfoliation of the bulk in DMF and evaluate its tribological properties as an additive to the paraffin oil under widely different conditions to those of the above work in the boundary lubrication regime using standards ASTM D4172 (392 N load, time 1h, 1200 rpm, temperature 75 ^oC) and ASTM D5183 (Step loading of 98 N at 10 min interval after running at 392N for 1h till failure of the lubricant) on a four-ball tribo-tester. The tribological activity data of V_2O_5 nanosheets can be very well compared with our results of rGO, g-C_3N_4, and MoS_2 because the tests were performed on the same machine under similar conditions and the same oil.

Further, the tribological performance of the aforementioned nanosheets rGO, g-C_3N_4, and MoS_2 has been upgraded by forming nanocomposites [Jaiswal et al. (2016), Verma et al. (2019), Verma et al. (2020), Singh et al. (2021), Shukla et al. (2020)] with different materials; likewise, the same may happen to V_2O_5 nanocomposites. The nanocomposite of V_2O_5 with PANI has already found an illustrious place in several fields, such as zinc-ion storage [Liu et al. (2020)], lithium-ion batteries [Chen et al. (2010)], ammonia gas sensors [Santos et al. (2019)], and microbial fuel cells [Ghoreishi, et al. (2014)], etc. due to its electrical conductivity, dielectric behavior [Islam et al. (2013)], electrochromic performance [Zhang et al. (2018)] microwave shielding and anticorrosion properties [Maruthi et al. (2021)]. Besides this, the importance of PANI, as stated above, has been admitted in the field of lubrication. Therefore, the present investigation explores the possibility of enhancing antiwear/antiwear efficiency and

load-carrying properties of the as-prepared V_2O_5 nanosheets by interacting with PANI. Thus, polyaniline intercalated vanadium pentoxide nanosheets were synthesized hydrothermally using in situ oxidative polymerization of aniline by oxidant V_2O_5. The V_2O_5 nanosheets, PANI, and the nanocomposite (PVO) have been studied by p-XRD, HR-SEM, TEM, and XPS. Their tribological performance in paraffin oil was compared based on ASTM D4172 and ASTM D5183 tests on a four-ball tester.

5.1 Materials and Methods

5.1.1. Chemicals

The required chemicals such as vanadium pentoxide powder (CAS No. 1314-62-1), potassium dichromate (CAS No. 7778-50-9), N, N-dimethylformamide (CAS No. 68-12-2), aniline (CAS No. 62-53-3), hydrochloric acid (CAS No.7647-01-0), and sulphuric acid (CAS No. 7664-93-9) were purchased from Sigma-Aldrich chemical Pvt. Ltd., Bangalore, India. Paraffin oil was obtained from Qualigens Fine Chemicals.

5.1.2. Preparation of lubricant additives

5.1.2.1. Preparation of V_2O_5 nanosheets

Preparation of V_2O_5 nanosheets has been achieved ultrasonically through N, N-dimethylformamide (DMF) exfoliation method. Bulk V_2O_5 powder (0.2 g) and 400 mL of DMF were mixed in a 500 mL beaker with constant stirring at room temperature for 12h, followed by sonication for three days. After that, the reaction mixture was kept for sedimentation, and the supernatant liquid was centrifuged to obtain exfoliated V_2O_5. The nanosheets were collected, washed with ethanol repeatedly to detach unused DMF, and finally dried at 70 °C for 10 h in a vacuum [Ganganboina et al. (2018)].

5.1.2.2. Preparation of polyaniline

Aniline was polymerized in an acidic medium using oxidant potassium dichromate. For the polymerization of aniline, 50 ml (0.1 M, 0.27 ml) sulfuric acid was added to 50 ml of (0.1 M, 0.46 ml) aqueous aniline. The reaction vessel was placed on a magnetic stirrer. 20 ml aqueous solution of potassium dichromate ($K_2Cr_2O_7$) oxidant (0.04 M, 0.24 g) was added using a dropping funnel. After the polymerization reaction was over, the final product was filtered, washed with dilute sulfuric acid, and dehydrated at 60 ^oC for 12 h in a vacuum. The synthesized polyaniline was finely ground, and the green powder was obtained [Vivekanandan et al. (2011)].

5.1.2.3. Preparation of PVO nanocomposite

For the preparation of the PVO, aniline was acidified to yield anilinium cations which were allowed to intercalate within exfoliated V_2O_5 nanosheets. The in situ oxidative polymerization of anilinium cations was brought about hydrothermally by oxidant V_2O_5 nanosheets. Vanadium pentoxide (0.18 g) and aniline (0.06 g) were taken in 40 mL of distilled water and stirred for 15 min. Then hydrochloric acid was added dropwise to the orange-colored reaction mixture until pH was maintained as 3. After 15 min sonication, it was transferred into a 50 mL Teflon autoclave, and the reaction was carried at 120 ^OC for 24 h. After the dark green product cooled down to room temperature, it was rinsed with a 1:1 ethanol-water mixture and dehydrated at 60 °C for 12h in a vacuum [Pang et al.(2005)] (**Fig. 5.1**).

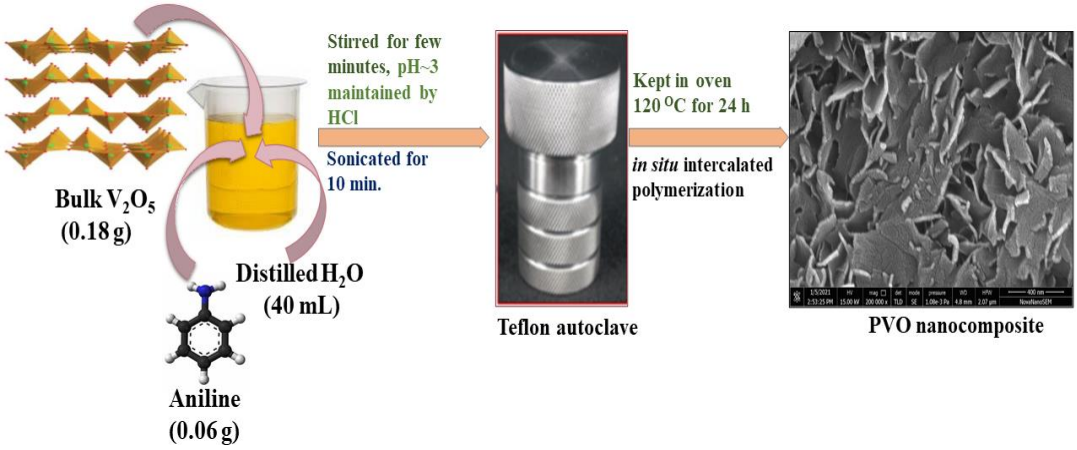

Fig. 5.1. Schematic in situ preparation of PVO nanocomposite

5.1.3. Procedure for Tribological activity tests

For testing, the samples were prepared by 1h sonication of the lubricant additives in paraffin oil (PO), having concentrations 0.000, 0.025, 0.050, 0.075, and 0.100 % w/v. Antiwear tests were conducted for all the test samples according to ASTM D4172 standards on a four-ball tribo-tester. From the observed data, 0.05 % w/v was established as the optimized concentration of the additives. Load ramp tests were carried out following ASTM D5183 conditions.

5.2. Results and discussion

5.2.1. Characterization of the prepared lubricant additives

The as-prepared additives have been characterized by p-XRD, SEM/HR-SEM, TEM/HR-TEM, FTIR, UV-visible and XPS. For morphological studies, HR-SEM images of the additives were taken. **Fig. 5.2(a-c)** exhibits HR-SEM images of V_2O_5 nanosheets, PANI nanorods, and

nanocomposite, respectively. **Fig. 5.2a** shows the nano lamellar structure of V_2O_5. The lateral size of nanosheets was found in the 200-250 nm range with a thickness of 7-10 nm. Therefore, nanosheets could easily access the rubbing surfaces [Yi et al. (2018)]. The chains of rod-like PANI are visible in **Fig. 5.2b**. The average diameter of rod-like PANI could be obtained between 65-70 nm. The PVO, **Fig. 5.2c**, shows intercalated PANI within the lamellar morphology of V_2O_5, having a thickness in the range of 10-20 nm. The EDX spectra of V_2O_5 and PANI, and PVO presented in **Fig. 5.3** show well-defined peaks for the constituent elements supporting the formation of the respective additives.

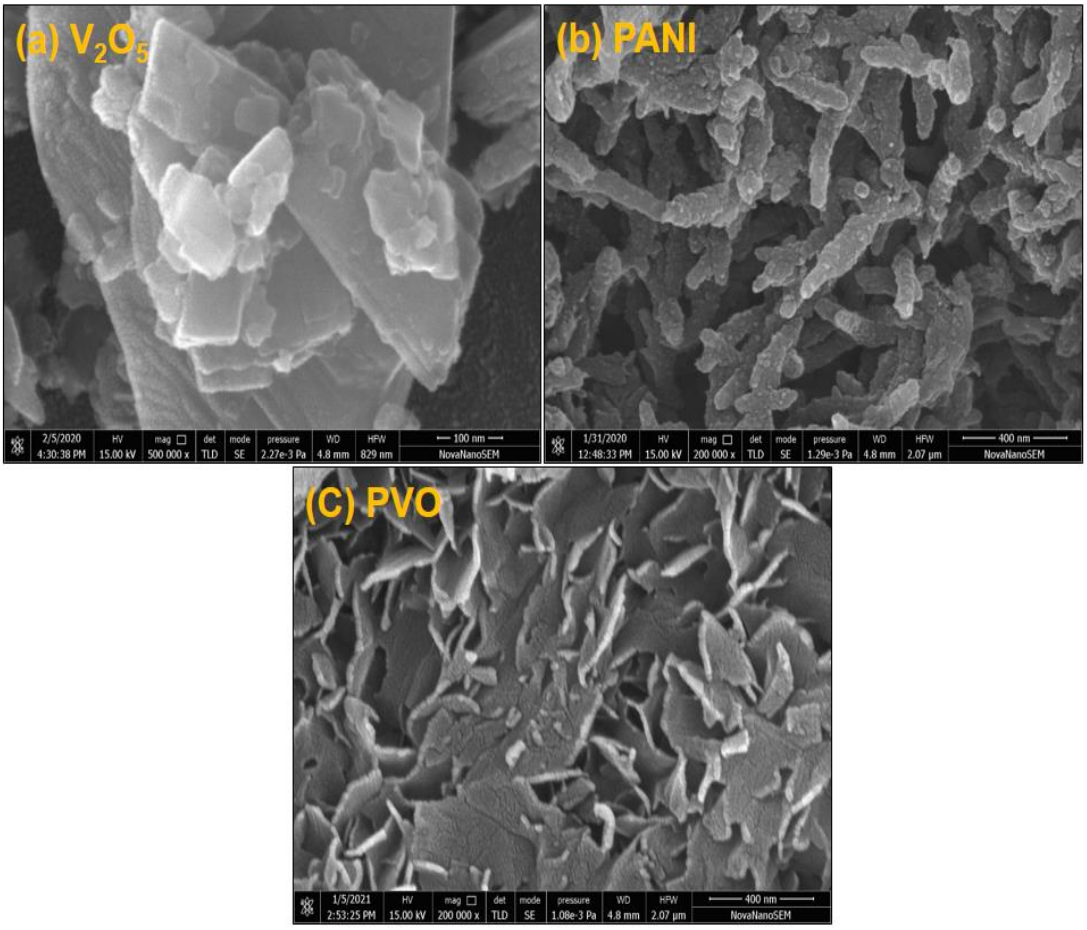

Fig. 5.2. HR-SEM images of (a) V_2O_5, (b) PANI and (c) PVO

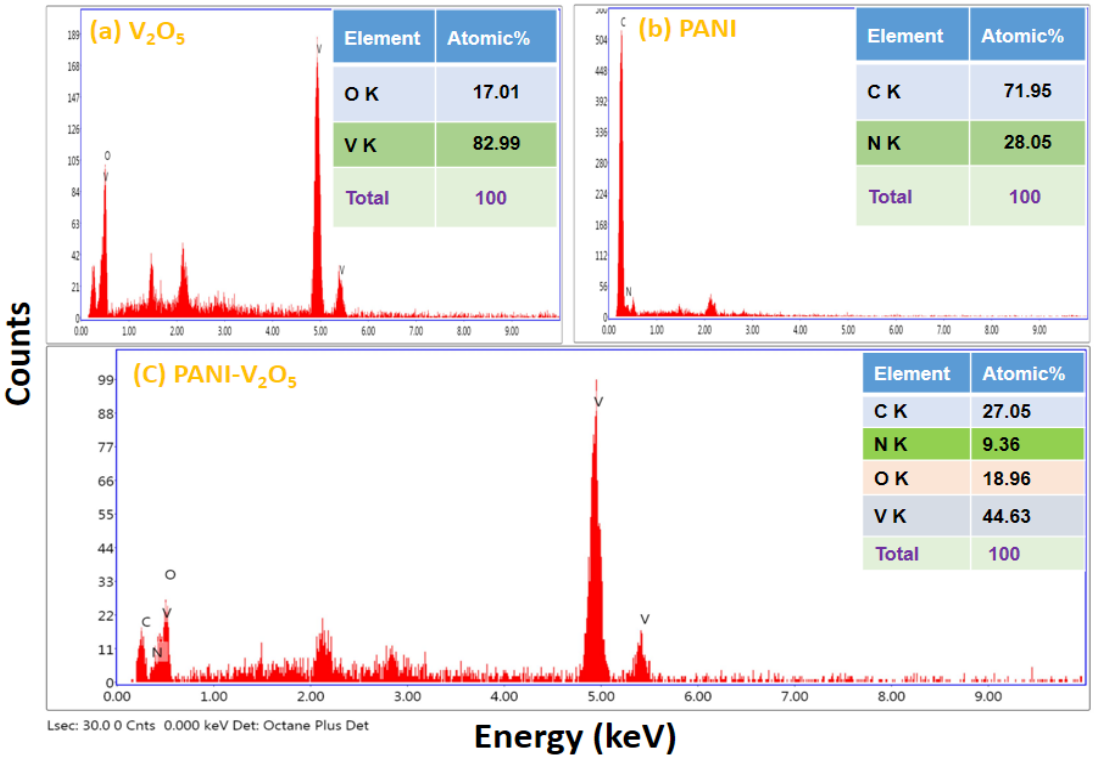

Fig. 5.3. EDX spectrum of V_2O_5, PANI, and PVO

TEM images of V_2O_5, PANI, and PVO, **Fig. 5.4(a-c)** have also been collected to inspect morphology critically. The nanosheet structure of V_2O_5 is clearly visible in **Fig. 5.4a**. The rod-like PANI with 65-70 nm width is identified in **Fig. 5.4b**, while PANI intercalated V_2O_5 nanosheets are apparent in **Fig. 5.4c**. **Fig. 5.4 a_1** illustrates an HR-TEM image of V_2O_5 nanosheets with 0.43 nm interplanar distance corresponding to the (001) plane [Kundu, et al. (2017)]. The selected area diffraction pattern (SAED) in the inset shows a crystalline structure. The semi-crystalline nature of polyaniline could be discerned from the SAED pattern, **Fig. 5.4 b_1**. The crystallinity of PANI depends on the reaction conditions [Kundu et al. (2017)]. **Fig. 5.4 c_1** portrays the HR-TEM of PANI intercalated V_2O_5 nanosheets, where the lattice fringes

corresponding to the (001) plane are clearly observed. The interlayer spacing of the (001) lattice plane of V_2O_5 nanosheets has increased substantially to 1.35 nm in the PVO showing strong interaction between components. Sufficient crystallinity can be inferred from the SAED pattern in the inset [Kundu, et al. (2017)].

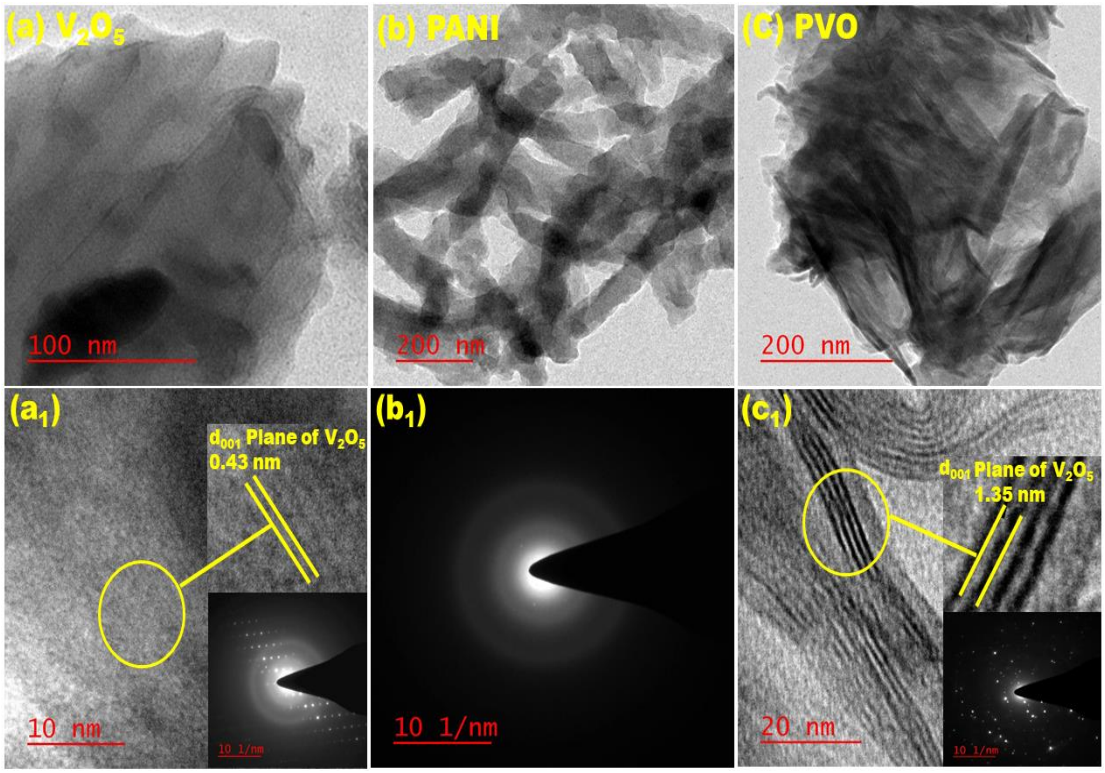

Fig. 5.4. TEM images of (a) V_2O_5, (b) PANI, (c) PVO, and (a_1) HR-TEM image of V_2O_5, (b_1) SAED pattern of PANI, (c_1) HR-TEM image of PVO. The inset in (a_1 and c_1) provides the SAED pattern of the additives

Fig. 5.5a portrays the XRD patterns of the precursor V_2O_5 powder, PANI nanorods, and PVO. The XRD of PANI shows broadband (15-30^o) with weakly resolved peaks implying a semicrystalline state [Vivekanandan et al. (2011)]. The XRD pattern of precursor V_2O_5 was confirmed by V_2O_5 (JCPDS 41-1426). All the diffraction peaks are indexed and assigned to the orthorhombic crystalline phase [Kundu, et al. (2017), Pang et al. (2005)]. The interlayer distance of the (001) plane was calculated as 0.43 nm [Rui et al. (2013)]. The PVO exhibits lower intensity peaks than V_2O_5 powder, corroborating the intercalation of PANI within the layered phase of V_2O_5 [Pang et al. (2005)]. The strongest peak corresponding to (00l) reflections for the lamellar V_2O_5 is slightly shifted to a lesser angle of 6.2^o. The characteristic peaks of V^{+4} oxide are also identified in the diffraction pattern of the PVO according to (JCPDS 81-2392). Notably, the interlayer distance has increased from 0.43 nm to 1.35 nm, confirming the phase transition from orthorhombic to monoclinic [Kundu et al. (2017)]. Some of the V^{5+} ions are reduced to V^{4+} ions during synthesizing the composite, where aniline gets oxidatively polymerized to polyaniline. These V^{4+} ions are supposed to play the role of polymerization initiators [Kundu et al. (2017)].

Fig. 5.5b depicts the FTIR spectra of the additives. The IR spectrum of V_2O_5 exhibits two characteristic stretching vibrational modes at 1022 cm^{-1} and 831cm^{-1} corresponding to νV=O and νV-O-V, respectively, and a vibrational bending mode at 609 cm^{-1} for V-O-V bridges [Dimitrov et al. (1994)]. Some absorption bands are observed in the IR spectrum of PANI at 3445 cm^{-1}, 3225 cm^{-1}, 1568 cm^{-1}, 1493 cm^{-1}, 1289 cm^{-1}, 1144 cm^{-1}, and 820 cm^{-1} corresponding to νN–H, νN–$H^{+\bullet}$, νC=C (quinoid ring), νC=C (benzenoid ring), νC–N(benzenoid ring), νC–N (quinoid ring) and out-of-plane C–H bending of the *p*-disubstituted

benzene ring, respectively [Srinivasan et al. (2018), Shumaila et al. (2011)].

In addition, νO–H for the water is observed as broadband along with νN–H [Singh et al. (2021), Kong et al. (2017)]. The existence of these peaks in the IR spectrum of the PVO supports the continuance of the characteristic structure of PANI in the nanocomposite. However, a slight shift in the position of bands suggests the interaction between PANI and V_2O_5 in the PVO.

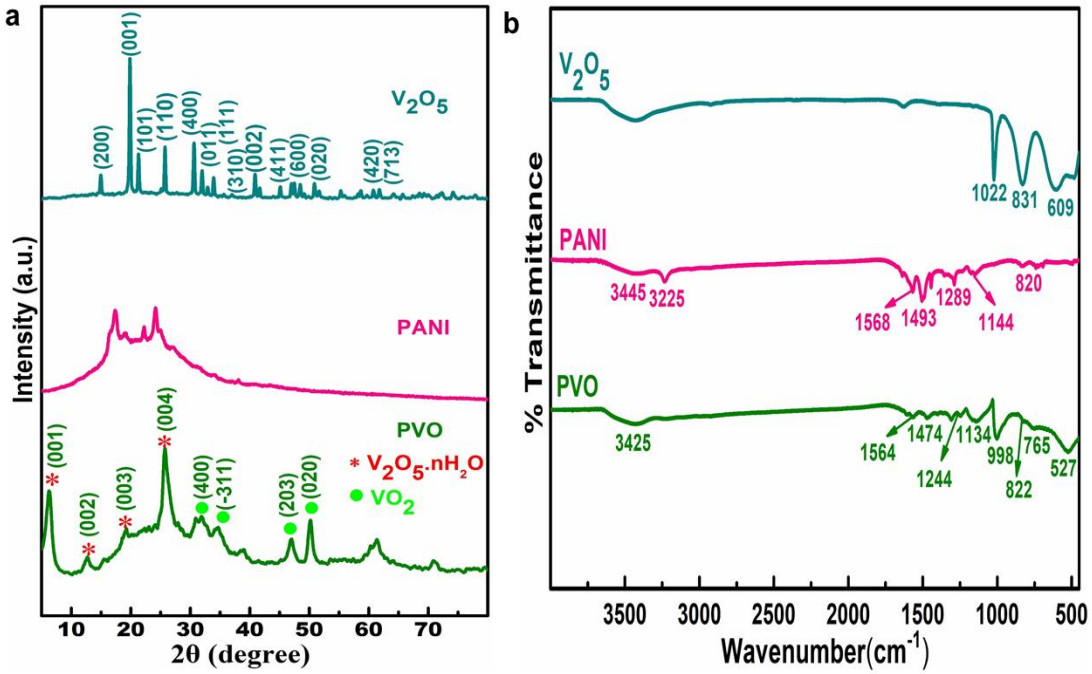

Fig. 5.5. (a) XRD patterns of V_2O_5 powder, PANI, and PVO (b) FTIR spectra of V_2O_5, PANI, and PVO

The ν(V=O) appearing at 1022 cm^{-1} in V_2O_5 nanosheets shifts to 998 cm^{-1} in the PVO, suggesting its involvement in intermolecular hydrogen bonding HN(PANI)……O-V (V_2O_5) [Chen et al. (2020)]. Thus, intercalated PANI props up the composite structure through hydrogen bonding type of non-covalent interactions in addition to van der Waals forces.

The chemical states of the contributing elements of the PVO could be identified by XPS. Peak fitting software was utilized for deconvoluting the core level spectra. Deconvoluted XPS spectra of C 1s, N 1s, O 1s, and V 2p are presented in **Fig. 5.6**. The core-level spectrum of C 1s illustrated in **Fig. 5.6a** divulges three peaks with binding energies 284.5, 285.2, and 286.6 eV corresponding to C-C/C=C/C-H, C-N/C=N bonds, and $\pi-\pi^*$ transitions, respectively [Kavita et al. (2020), Kavita et al. (2020), Golczak et al. (2008)]. The N 1s spectrum, depicted in **Fig. 5.6b**, exhibits three peaks at binding energies 399.5, 400.5, and 401.6 eV for quinoid phenyl ring, benzenoid ring, and quaternary ammonium, respectively [76]. The peaks observed at 530.1, 530.8, and 532.6 eV in the O1s spectrum **Fig. 5.6c** are attributed to the V-O bond and V $2p_{3/2}$ satellite and water, respectively [66]. The V2p core-level spectrum in **Fig. 5.6d** exhibits four peaks at binding energies 516, 517.3, 523.6, and 524.8 eV assignable to V^{+4} $2p_{3/2}$, V^{+5} $2p_{3/2}$, V^{+4} $2p_{1/2}$ V^{+5} $2p_{1/2}$, respectively [Kundu et al. (2017)]. Based on XPS spectra, it can be inferred that there is no chemical interaction between PANI and V_2O_5 in the PVO.

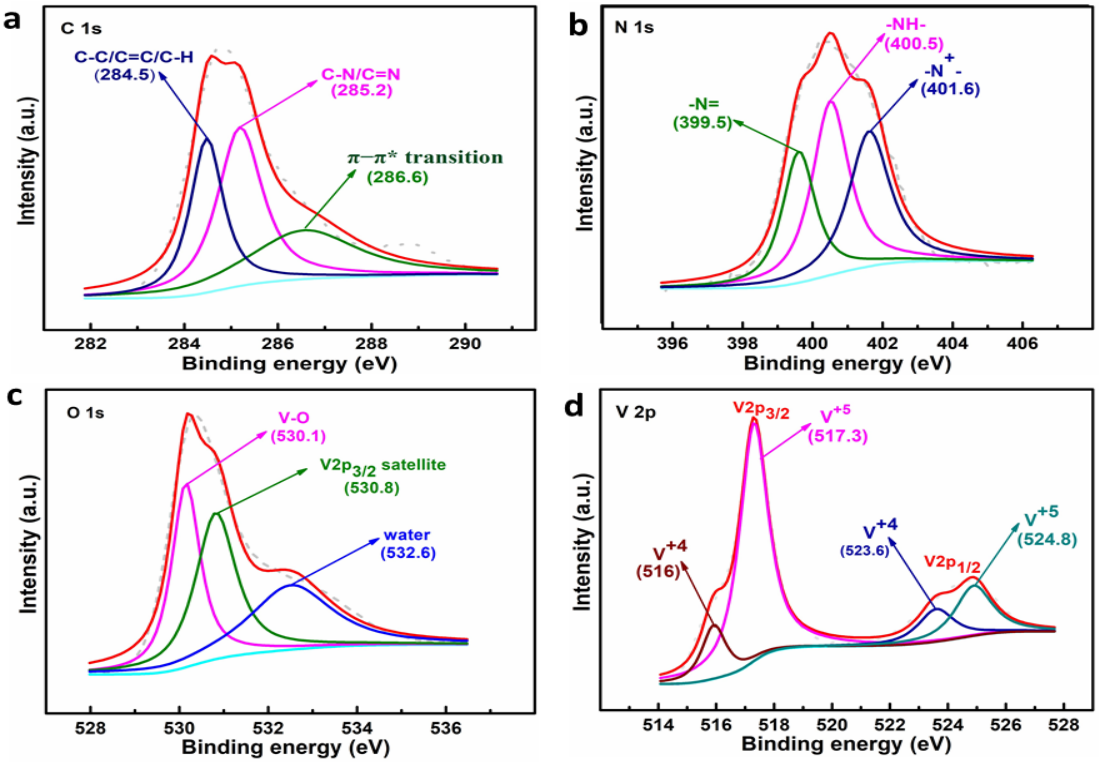

Fig. 5.6. Deconvoluted XPS images of PVO nanocomposite

5.2.2. Tribological Properties

5.2.2.1. Stability of admixtures dispersed in paraffin oil

For tribological properties, the stability of dispersions of nano additives is, indeed, necessary. The dispersion stability of the investigated formulations was studied by UV/visible spectroscopy using ten-fold PO diluted optimized concentration (0.05 % w/v) of the additives within 48 h. The UV-Vis spectra of additives in the range 260-800 nm are provided in **Fig. 5.7**.

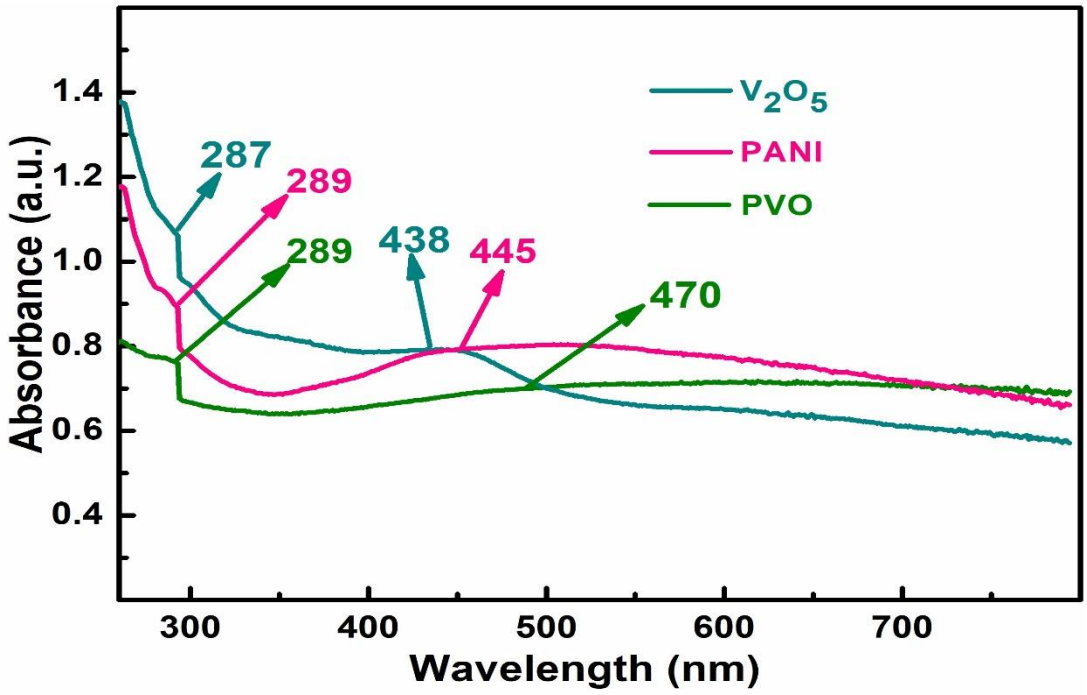

Fig. 5.7. UV-Vis spectra of additives

The absorption spectrum of V_2O_5 shows two intense bands at 287 nm and 438 nm, assignable to the electronic transition O (2p) to V (3d) and the bandgap of V_2O_5, respectively [Kundu et al. (2017)]. PANI spectrum is characterized by two absorption bands at 289 and 445 nm corresponding to π-π* transition in the benzenoid ring and polaron-π* transition in the emeraldine salt (ES) respectively [Bhadra et al. (2007)]. In the case of the PVO, two absorption bands could be identified at 289 and 470 nm. The latter band, in fact, has undergone a redshift. The absorbance values of the PVO in the range 260-800 nm from zero to 48 h at 12 h intervals are separately shown in **Fig. 5.8a** (inset view). **Fig. 5.8a** illustrates the variation of relative absorbance of the additives against settling time. The relative absorbance, as expected, reduces with time for all additives; however, the magnitude of reduction is the least in the case of the

PVO showing high stability. **Fig. 5.8b** displays photographs of blends of all the additives in PO initially and after every12 h interval up to 48 h showing minimum settling in the case of the PVO.

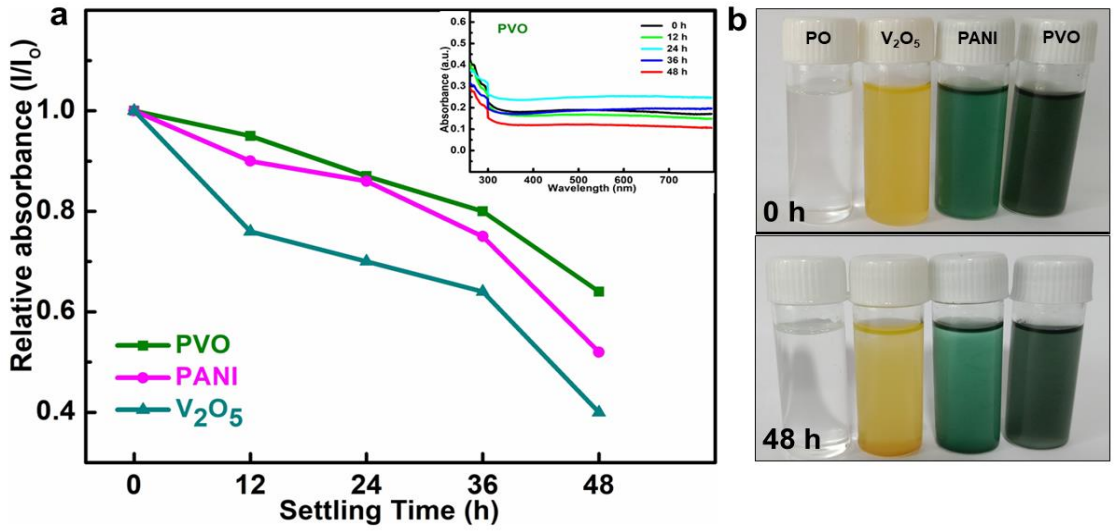

Fig. 5.8. (a) Dispersion stabilities of paraffin oil containing V_2O_5, PANI, and PVO by UV−vis spectrophotometry, (b) optical photographs of the additives dispersed in paraffin oil at 0 h and 48h

5.2.2.2. Wear and friction studies (ASTM D4172Test)

The concentration is a critical parameter that influences the tribo-activity of the additives. **Fig.5.9a** depicts the results of the antiwear test as per ASTM D4172 test conditions showing how the mean wear scar diameter (MWD) varies with the concentration of the additives. Compared to base oil, MWD decreases considerably in the presence of all blends of additives. There is a remarkable decrease in MWD value up to 0.050 % w/v in every case.

Afterward, it rises visibly for all the additives. The concentration 0.05 % w/v has finally been taken as the optimized concentration. It can be noted that the optimized concentration for nano lamellar V_2O_5 is much smaller than the other nanosheets from our research group, rGO [Verma et al. (2019)], g-C_3N_4 [Singh et al. (2021)], and MoS_2 [Shukla et al. (2020)] showing its excellent performance. Further out of the tested additives in the present investigation, MWD for any of the tested concentrations is minimum for the PVO; therefore, it turns out to be the best additive.

Fig. 5.9b displays the variation of coefficient of friction (COF) vs. concentration of the additives. The COF is very high for plain PO; however, it reduces adequately in the presence of additives. Evidently, at the concentration of 0.025 % w/v, COF values are lowered in each case. The lowering continues till 0.050 % w/v. At the next concentration, 0.075 % w/v COF increases for all the additives. Up to this concentration, COF is the lowest for the PVO. For the last concentration, 0.100 % w/v, although there is an increase in COF in the case of PVO, for PANI and V_2O_5 considerable decrease is observed. Thus, the minimum value of COF for the PVO (0.04798) is observed at 0.050 % w/v; however, for V_2O_5 (0.0590) and PANI (0.05162), it is obtained at 0.100% w/v.

The antiwear and antifriction efficacy of different additives in base oil has been determined using ASTM D4172 test conditions. The test results are depicted in the form of a bar diagram **(Fig. 5.9c)**, where MWD data and COF have been displayed simultaneously at the concentration of 0.05% w/v. The MWD value for PO is 0.735 mm; the decrement in MWD in the presence of additives directly relates to their antiwear behavior. In the case of nano lamellar V_2O_5, the MWD has reduced to (22.4%), but for other reported nanosheets, rGO [Verma et al.

(2018)], g-C_3N_4 [Singh et al. (2021)], MoS_2 [Shukla et al. (2020)], MWD reduction is much lesser, showing its greater antiwear efficiency. Furthermore, the MWD reduction has been observed for other tested additives, too, PANI (26.3 %) and PVO (31.3%). Thus, the PVO shows improved antiwear performance compared to PANI or V_2O_5 nanosheets.

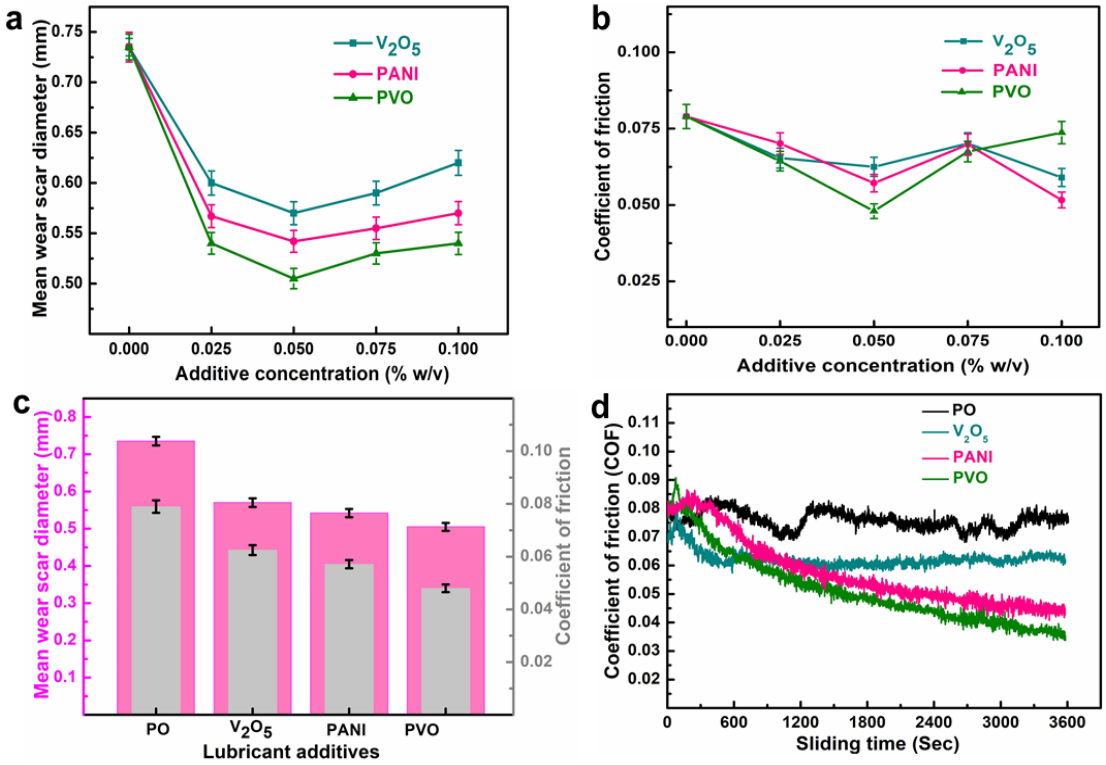

Fig. 5.9. ASTM D 4172 test for PO with and without additives, (a) Optimization of the concentration of nano additives, (b) Alteration of COF vs. nano additives concentration, (c) Bar diagram showing average COF and MWD, (d) Alteration of the COF with sliding time

The variation of COF of PO with and without additives vs. time is displayed in **Fig. 5.9d**. As expected, the COF value is high initially in each case because tribochemical interaction has not yet started to form tribofilm. With time tribofilm is created, resulting in stabilized COF. The average COF value of PO, 0.0790, undergoes a reduction in the presence of V_2O_5 nanosheets (21.0 %). The COF reduction for V_2O_5 is superior to rGO [Verma et al. (2018)], it is inferior to g-C_3N_4 [Singh et al. (2021)] and MoS_2 [Shukla et al. (2020)], indicating greater antifriction efficiency than rGO but lower than g-C_3N_4 and MoS_2. The observed behavior for V_2O_5 may be because of its hardness. For other investigated additives, friction reduction was noted as PANI (27.7 %) and PVO (39.4 %), consequently, the antiwear efficiency of PVO has enhanced compared to V_2O_5 and PANI.

5.2.2.3. Load ramp test (ASTM D5183 test)

For determining the load-bearing capacity of PO and its admixture with additives, the test was conducted for the optimized concentration of the additives following the conditions 392 N load, 600 rpm, 75°C temperature, and 60 min duration. Thus, the running-in period was completed. Further continuance of the steady-state test was carried out by successively adding 98 N load every 10 min till the seizure load when balls are seized due to exorbitant frictional torque. The seizure load corresponds to the failure of the lubricant to bear the load. **Fig. 5.10** reveals the deviation of frictional torque against stepwise loading and time for PO alone and its blends with additives. It is evident from the Figure that PO fails at 1078 N load. PO blended with V_2O_5 nanosheets fails at a higher load, 1568 N; the seizure loads for other nanosheets, rGO [Verma et al. (2018)], g-C_3N_4 [Singh et al. (2021)], MoS_2 [Shukla et al. (2020)] are much lower,

indicating the higher load-carrying capacity of V_2O_5. The seizure loads for the blends of PANI (2352 N) and the PVO (2744 N) are notably greater than V_2O_5. The remarkably enhanced load-carrying ability of PVO adds to its significance.

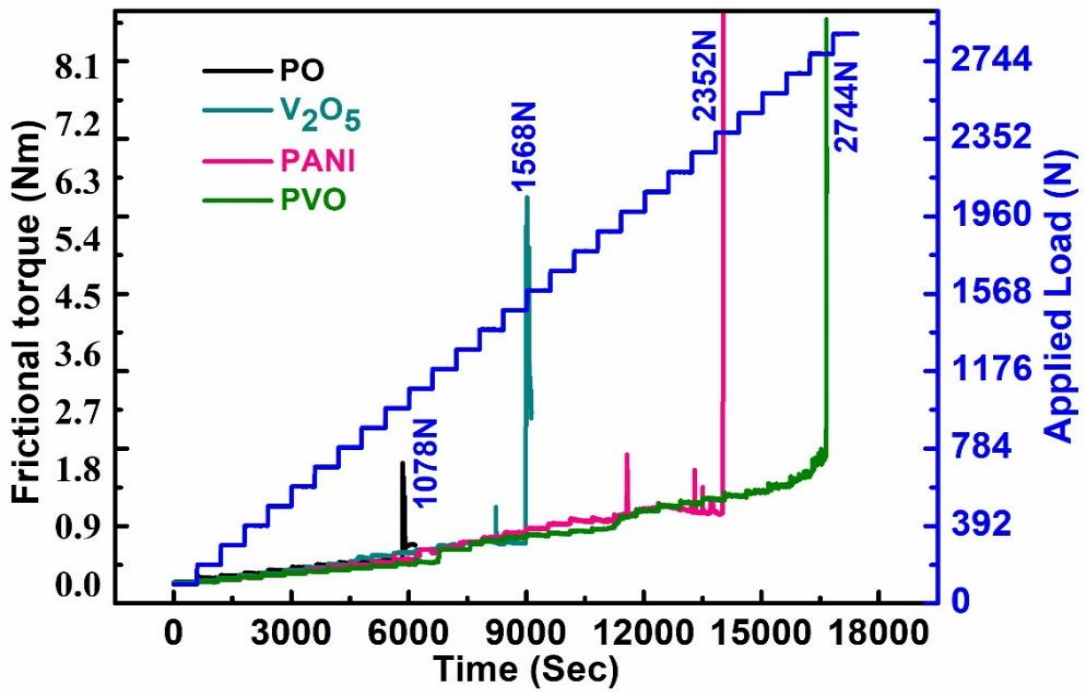

Fig. 5.10. Alteration of frictional torque with stepwise loading and time for different additives at an optimized concentration, 0.05% w/v under ASTM D5183 test conditions

5.2.2.4. Frictional power loss (P)

The frictional power loss was computed for PO and its blends. Maximum consumption of power (0.0628 MJ) occurs for PO alone. However, it declines appreciably for blends, 0.0497 MJ for V_2O_5, PANI (0.0410 MJ), and PVO (0.0381 MJ). Hence, it was observed from the above-provided data **(Table 5.1)** that minimum energy is consumed in the case of PVO.

Table 5.1. Frictional power loss measurement for different additives at an optimized concentration, 0.05 % (w/v) in paraffin oil

S.N.	Additives	Power consumption (MJ)	Reduction in Power consumption	% Reduction in Power consumption
1.	PO	0.0628	____	____
2.	V_2O_5	0.0497	0.0131	21.0
3.	PANI	0.0410	0.0218	35.0
4.	PVO	0.0381	0.0247	39.4

5.2.2.5. Characterization of worn surfaces

Morphological studies of the wear track have been conducted by SEM and AFM of the ball surface lubricated with PO (base oil) with and without additives at an optimized concentration (0.05% w/v) after the ASTM D4172 test. The SEM images are provided in **Fig. 5.11** (a-d). In the presence of plain oil, the surface appears highly corrugated. On the contrary, blends of additives with PO significantly amend the surface. The extent of the amendment of the surface follows the antiwear properties of the investigated blends. The values of MWD are mentioned in the inset of the figure; PO; 0.735 mm, V_2O_5; 0.570 mm, PANI; 0.542 mm and PVO; 0.505 mm, which matches precisely with the smoothness of the worn surface. The EDX spectrum of the worn surface in the presence of the PVO (**Fig. 5.11d$_1$**) divulges the existence of all elements forming the nanocomposite providing evidence in favor of adequately adsorbed additive on the wear track.

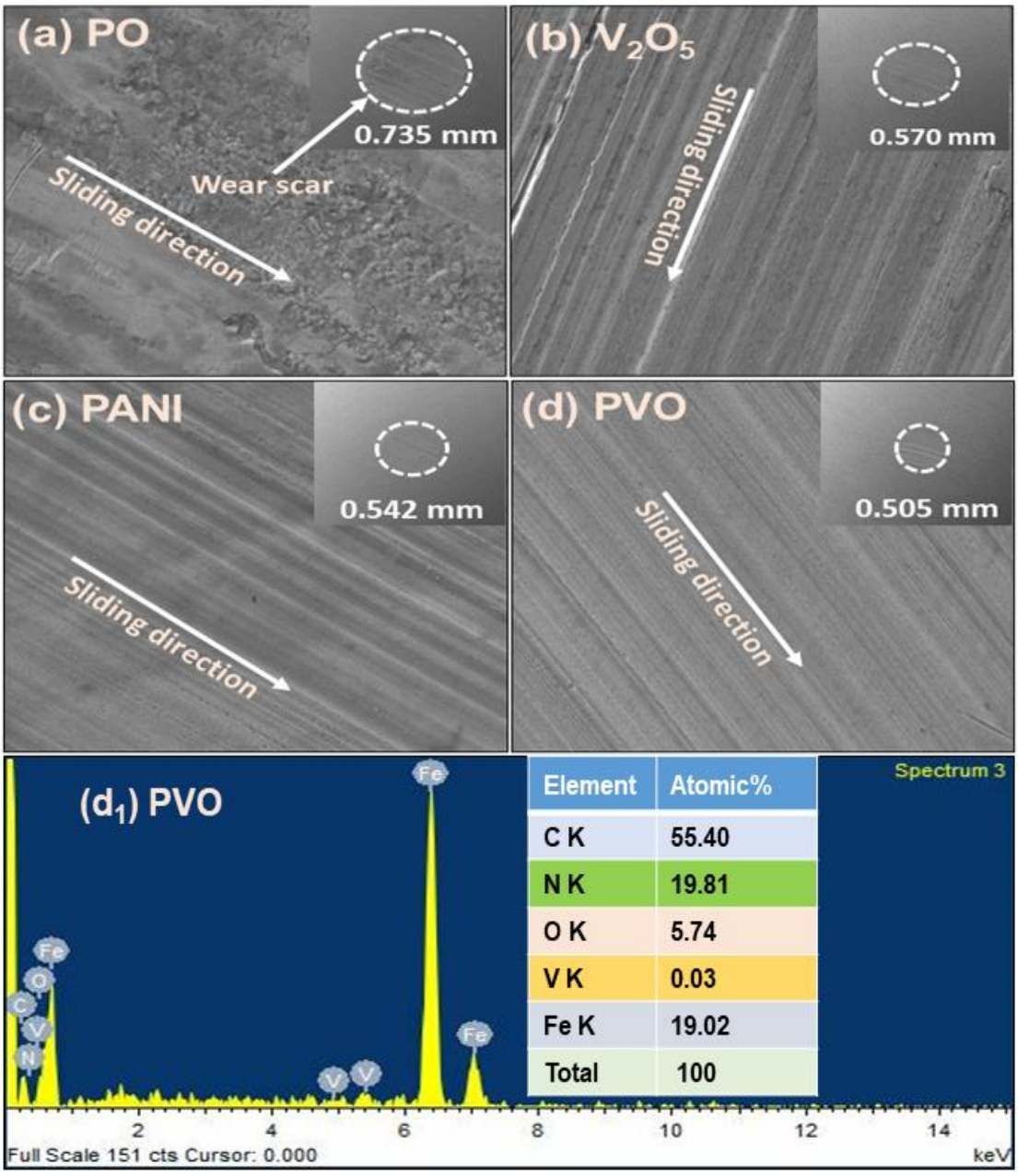

Fig. 5.11. SEM (a-d) images (inset: full view of the wear scar at 100× and wear scar surface at 2.00K× magnification) of the worn steel surface lubricated with paraffin oil in the presence and absence of additives (0.05 % w/v) under ASTM D4172 test conditions and (d_1) EDX spectrum of the worn steel surface lubricated with PVO

Furthermore, the 3D-AFM images of the wear scar are presented in **Fig. 5.12** (a-d), along with surface roughness data, area roughness (Sq), and line roughness (Rq). A noteworthy decline is evident in the Rq and Sq values from plain oil to the blends. Visibly, the surface becomes relatively even in the case of the PVO.

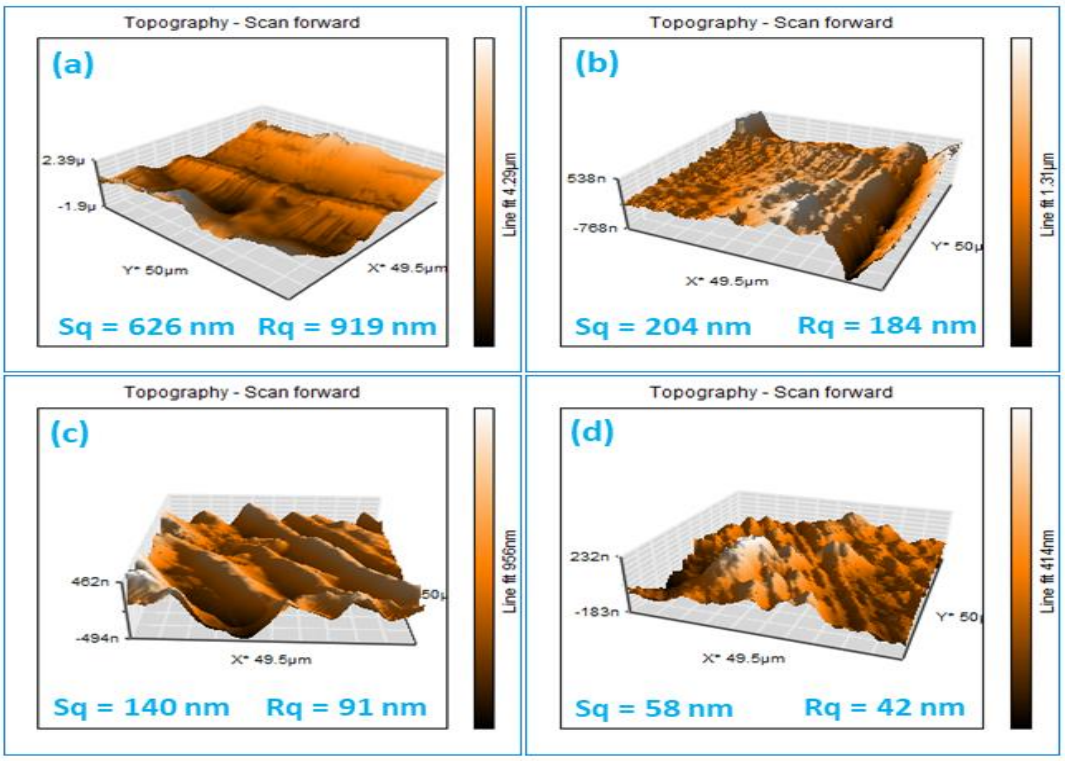

Fig. 5.12. AFM (*3D*) images of the worn steel surface lubricated with different additives (0.05 % w/v) in base oil after ASTM D4172 test: (a) PO; (b) V_2O_5; (c) PANI; (d) PVO

After the antiwear test, the XPS spectra of the wear scar surface lubricated with PO containing the PVO were taken. The inherent tribofilm developed in situ was analyzed for the

chemical states of the elements. **Fig. 5.13**(a−e) depicts the deconvoluted core-level spectra of C 1s, O 1s, N 1s, V 2p, and Fe 2p based on peak fit software. The C 1s spectrum shows only two peaks with binding energies 284.6 and 285.1 eV regarding C-C/C=C/C-H, and C-N/C=N, respectively [Kavita et al. (2020)]. The third peak representing the π−π* transition has disappeared due to the rupture of the polyaniline chain. The N 1s and O 1s spectra remain almost unaffected in the tribofilm.

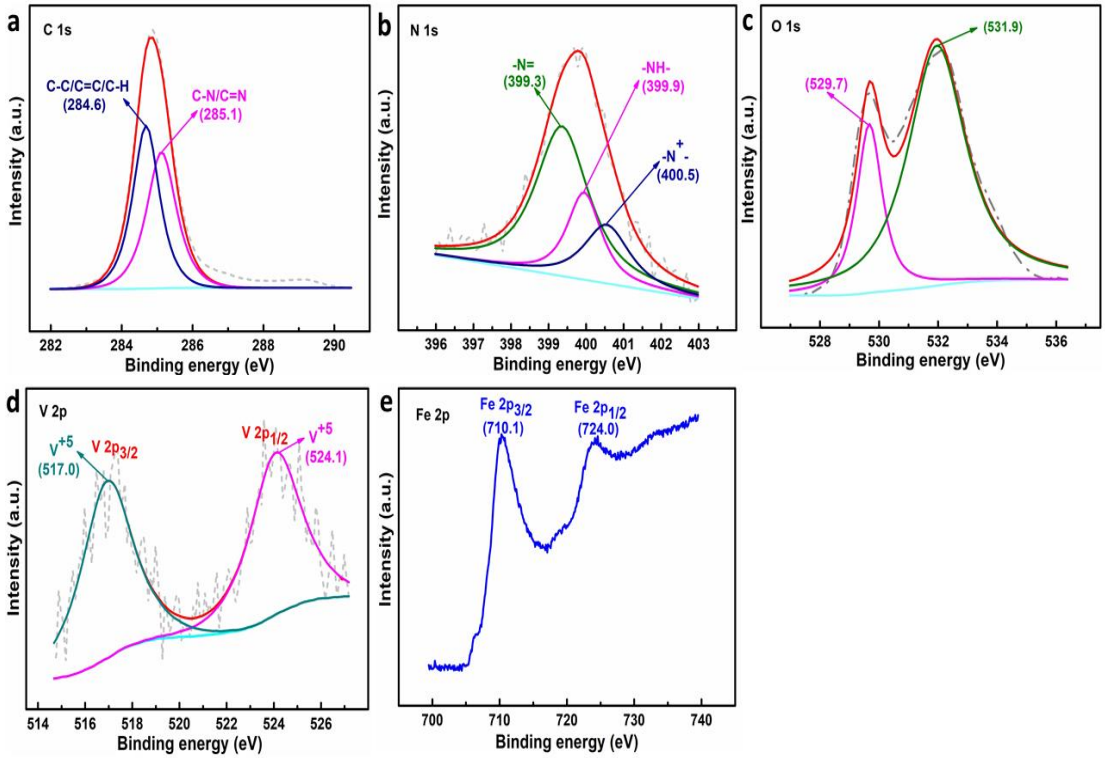

Fig. 5.13. Deconvoluted XPS spectra of the tribofilm formed on the steel surface lubricated with the PVO nanocomposite under ASTM D4172 test conditions: (a) C 1s spectra, (b) N 1s spectra, (c) O 1s spectra, (d) V 2p spectra, and (e) Fe 2p spectra

The V 2p spectrum is characterized by two peaks at binding energies 517.0 and 524.1 eV of V^{+5} $2p_{3/2}$ and V^{+5} $2p_{1/2}$ states, respectively. There is no reminiscence of V^{4+} as it has oxidized during the test. The existence of peaks in the Fe 2p spectrum for Fe^{3+} $2p_{3/2}$ (710.1 eV) and $2p_{1/2}$ (724.0 eV) is indicative of the oxidation of ferrous ions to ferric ions in the course of the test [Verma et al. (2018), Shukla et al. (2020), Verma et al. (2020a)]. From XPS spectral studies, an inference may be drawn that the tribofilm is composed of V_2O_5, Fe_2O_3, and adsorbed organic species of PANI.

5.2.2.6. Tentative Mechanism of Lubrication

The nanosheets of V_2O_5 show inherent lubricity due to van der Waals forces existing between them, facilitating their movement over one another [Londero et al. (2010), Ranea et al. (2019)]. PANI, a conducting polymer, is very well known to show tribological activity [Liu et al. (2018)]. The splendid tribological activity of the PVO may be attributed to PANI intercalating between V_2O_5 (nanosheets). The inserted polyaniline between nanosheets of vanadium pentoxide prevents their agglomeration and averts their restacking strongly due to intermolecular hydrogen bonding NH .....O-V [Chen et al. (2020), Petkov et al. (2005)]. Substantial enhancement of interplanar spacing corresponding to the (001) plane of V_2O_5 authenticates its phase transformation from orthorhombic to monoclinic, indicating remarkable interaction between the nanosheets and PANI. Thus, a significant amount of synergy accounts for the tribological performance of high order for the composite. EDX analysis of the wear scar surface in the presence of the composite supports the presence of the C, N, O, and V as individual components of the additive in the tribofilm. The XPS studies verify the complete tribochemical oxidation of V^{4+} into V^{5+} and Fe^{2+} into Fe^{3+}. The oxides of vanadium (V_2O_5),

iron (Fe_2O_3), and the adsorbed products PANI compose the tribofilm. The firm and adherent nature of tribofilm indeed has enhanced the seizure load and lower friction/wear. The diagrammatic representation of the proposed lubrication mechanism is given in **Fig. 5.14**.

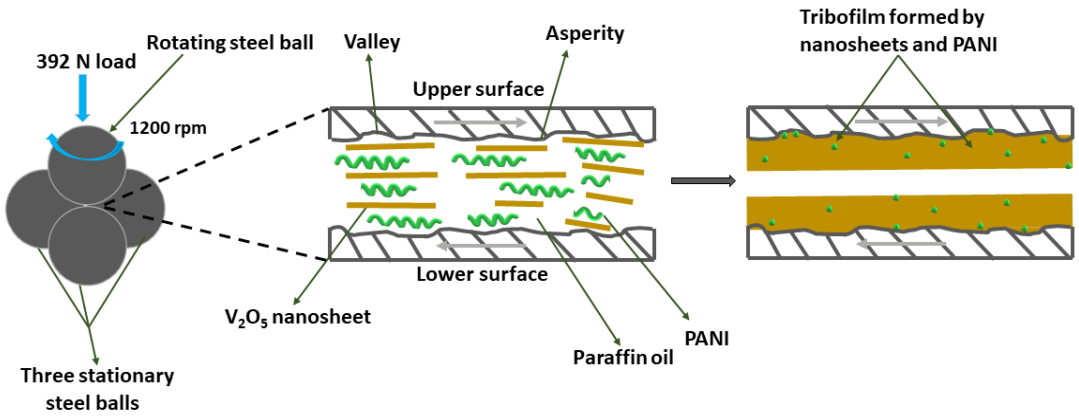

Fig. 5.14. Diagrammatic representation of the proposed mechanism of lubrication in the presence of nanocomposite PVO in paraffin oil

5.3. Conclusions

The tribological activity of V_2O_5 nanosheets was compared with our earlier results of rGO), g-C_3N_4, and MoS_2 nanosheets based on the parameters; mean wear scar diameter (MWD), coefficient of friction (COF) obtained from ASTM D4172 test, and seizure load from ASTM D5183 test using a four-ball tester. It could be ascertained that V_2O_5 behaves as the best antiwear agent with the lowest value for the optimized concentration. On the contrary, it is not that good friction reducer, only better than rGO. The load-carrying capacity of V_2O_5 and MoS_2

are similar, but those of rGO and g-C_3N_4 are much lesser. An attempt was successfully made to improve further the tribological properties of V_2O_5 nanosheets by grafting conductive polyaniline chains using *in situ* oxidative polymerization on V_2O_5, yielding the nanocomposite PANI-V_2O_5.nH_2O. Morphological studies of the composite by FE-SEM, TEM, and HR-TEM discern PANI intercalated into lamellar V_2O_5. Characterization of the additives was carried out by XRD and spectroscopic techniques, FT-IR and XPS. The observed data indicate the absence of covalent interaction between PANI and V_2O_5 in the PVO. However, the interaction is through non-covalent forces like hydrogen bonding between organic and inorganic components, NH (PANI).....O-V (V_2O_5), and van der Waals forces. The intercalation of PANI between V_2O_5 nanosheets is evidenced by the considerably enhanced interlayer spacing between the V_2O_5 nanosheets. The tribological tests divulged the outstanding improvement in the antiwear/antifriction efficiency and load-carrying capacity of the PVO. The improvement in tribological properties is attributed to synergistic interactions between V_2O_5 nanosheets and PANI. The feasibility of lubricating behavior of V_2O_5 nanosheets is apparently due to weak van der Waals forces existing between them, intercalation of PANI reinforced the structure, restricted agglomerating tendencies, and piling up the nanosheets using hydrogen bonding and van der Waals forces.